# Dynamics of the one-dimensional self-organized forest-fire model

Viktor Nagy and Edward Ott
*University of Maryland, College Park, Maryland 20742, USA*
(Received 27 February 2008; published 13 August 2008)

We examine the dynamical evolution of the one-dimensional self-organized forest-fire model (FFM), when the system is far from its statistically steady state. In particular, we investigate situations in which conditions change on a time scale that is faster than, or of the order of the typical time needed for relaxation. An analytical approach is introduced based on a hierarchy of first-order nonlinear differential equations. This hierarchy can be closed at any level, yielding a sequence of successively more accurate descriptions of the dynamics. It is found that our approximate description can yield a faithful description of the FFM dynamics, even when a low order truncation is used. Employing both full simulations of the FFM and our approximate descriptions, we examine the time scales and cluster-size-dependent dynamics of relaxation to the statistical equilibrium. As an example of changing external conditions in a natural forest, the effects of a time-dependent lightning frequency are considered.

DOI: 10.1103/PhysRevE.78.021113 PACS number(s): 05.90.+m, 05.65.+b, 05.45.Df

## I. INTRODUCTION

Over the last two decades, systems exhibiting self-organized behavior have attracted considerable attention. The term self-organized criticality (SOC) refers to extended dissipative systems that are driven into a critical, self-similar, and statistically stationary state independent of initial conditions, without the need to fine-tune the system parameters. Their common features can be characterized by slow driving energy input, with rare intense dissipation events, whose size distribution obeys a power law. Illustrating the versatility and applicability of SOC in nature, several examples have been identified. Sandpile models, which provide simple models for avalanches, have been investigated both numerically [1,2] and analytically [3]. Additional examples are earthquake models [4], diffusion-limited aggregation [5], and invasion percolation models [6]. Many properties of SOC systems compare favorably to experimental data. For instance, good quantitative agreement was found between the interoccurence time statistics of solar flares and the Bak-Tang-Wiesenfeld sandpile model [7].

In this paper our focus is the self-organized forest-fire model (FFM), originally introduced as a possible realization of SOC [8]. This model was later modified by introducing a lighting parameter to provide proper scaling behavior [9]. Computer simulations [9–11] and analytical considerations [12] confirm that sufficient separation of time scales leads to SOC in the FFM. Mean-field-theory approximations [13], an inverse-cascade model [14], and a renormalization group technique [15] were proposed as analytical approaches to understand the equilibrium of the FFM.

Previous work on the FFM has focused on understanding the statistically steady behavior. However, it is also of interest to examine situations where changes in the external conditions in these systems occur on a time scale that is faster than, or of the order of the typical time needed for relaxation to the statistically steady state. As examples, we mention the following situations of interest.

(1) The forest system on a large island might be destroyed or otherwise globally effected by the occurrence of some major disaster such as a large volcanic eruption. In such a case one might be interested in the time evolution of the regrowing forest including the effect of forest fires. Thus one might be interested in the FFM dynamics starting from an initial condition far from the statistically steady state.

(2) The global conditions of a forest might be effected by climate changes. If these changes occur on a time scale shorter than, or of the same order as, the relaxation time to the FFM statistically stationary state, then consideration of dynamical processes away from the relaxed state is required.

(3) Normal seasonal weather changes can occur on a time scale that is comparable to the frequency of large snow avalanches.

(4) Self-organized criticality also arises in scale-free networks [16] from local interactions of large numbers of individuals. For instance, one might be interested in the dynamics of a computer network in the case of sudden introduction of a new technology or of sudden introduction of new connections and nodes to the system.

(5) One might be interested in reducing the number of rare and particularly destructive large forest fires by controlling the system dynamics, e.g., by preventing the formation of large connected patches of forest through controlled burns. In such a case, intermittent application of controls can place the state away from the statistical equilibrium towards which it subsequently begins to relax. This is a problem we intend to address in the future.

In the present paper we investigate the *dynamical* behavior of the self-organized forest-fire model in one dimension, in the simplest case when burning of trees occurs instantaneously. The one-dimensional FFM is defined on a linear grid of $L$ sites, which for simplicity is taken to be periodic. Each site can be in either of two states: empty (no tree on the site) or occupied (there is a tree on the site). The state of the system is updated in discrete steps using the positive real parameters $p \ll 1, f \ll 1$. In each step a tree is placed on the empty sites with probability $p$. If a site is occupied, then we "hit it with a lightning bolt" with probability $f$, which makes it "burn down," turning it into an empty site. If we denote the time needed to burn down the largest clusters by $T_{\max}$ (a cluster is a group of contiguous trees), then critical behavior

 

in the FFM arises in the presence of double time-scale separation, $T_{\max} \ll p^{-1} \ll f^{-1}$ [19]. The condition $T_{\max} \ll p^{-1}$ is most easily realized when fire spreads instantaneously to every site that is part of the cluster containing a burning tree, which is the situation that we consider in the rest of this paper. A key parameter of the model is the ratio

$$\gamma = f/p, \tag{1}$$

which is assumed to be much less than one. Because the FFM is self-organized, it can be expected that any substantial departure from its equilibrium state will be followed by a relaxation process. Our goal is to understand how the dynamical behavior of the self-organized forest-fire model can be understood. As we shall see later, the time scale for relaxation to the statistically steady state is of the order of $1/p$ time steps. Thus the object of our paper is to study the FFM dynamical process on the $1/p$ time step scale. A hierarchy of steady-state equations for correlation functions of the FFM was proposed in [17], and solved, as an approximation, with a mean-field closure scheme. An inverse cascade model was examined in [14], which reproduces several characteristics of the FFM. In the present paper we develop a hierarchy of equations that describes the dynamics of the FFM and can be closed to produce a set of self-consistent equations at any arbitrary level, thus producing a sequence of successively more accurate approximate descriptions of the dynamics. We use these equations along with numerical simulations to examine the relaxation properties of the FFM and the effect of nonsteady external parameters of the model.

In Sec. II we present a discussion of the dynamics and examine an analytical approach for describing the nonequilibrium behavior of the one-dimensional FFM. In Sec. III we compare our analytical results with numerical simulations and discuss their validity. Finally, in Sec. IV we summarize our results and give conclusions.

## II. DYNAMICS OF THE FOREST-FIRE MODEL IN ONE DIMENSION

### A. Framework

The one-dimensional model we consider is defined on a grid consisting of $L$ sites with periodic boundary conditions. We now define what we mean by a "cluster." In Fig. 1 each box represents a site. There are $L=32$ sites shown, arranged on a circle, where the circular topology corresponds to the periodic boundary conditions of our model. An example of state is shown, where a symbol $T$ labels a site occupied by a tree, and a symbol $E$ labels an empty site. A cluster is a sequence of sites that are bounded by exactly one empty site on each side, and that has no empty sites in its interior. If there are two consecutive empty sites, we say that there is a cluster of size zero between them. Otherwise, the size of a cluster is defined as the number of trees between its bounding empty sites. For every $x \leqslant L$ we define

$$S_x = \text{number of clusters of size } x. \tag{2}$$

For example, in Fig. 1 cluster sizes are indicated by the numbers shown outside the circle of sites, and $S_5=1$, $S_4=1$, $S_2=4$, $S_1=1$, $S_0=7$. In general, since each empty site bounds two clusters (one on each side), and each cluster bounds two empty sites, the number of empty sites, denoted $N_e$, equals the number of clusters,

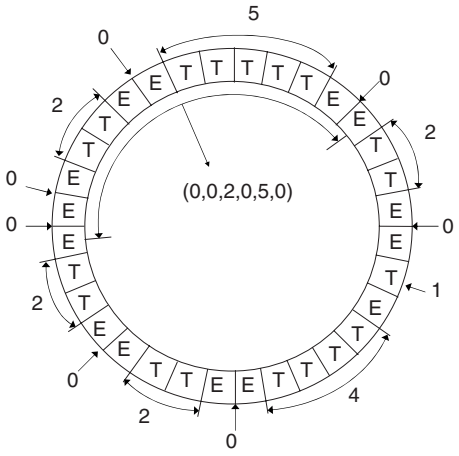


FIG. 1. A state of the FFM for $L=32$.

$$N_e = \sum_{x=0}^{L} S_x, \tag{3}$$

and the total number of sites can be expressed as

$$L = N_e + \sum_{x=0}^{\infty} x S_x. \tag{4}$$

As shown in Ref. [12] the statistically stationary $S_x$ follows a simple power-law distribution $S_x \sim x^{-2}$ for $\gamma x \ll 1$. As discussed in Sec. III A, statistical fluctuations of $S_x$ in time are always present in the FFM, but become smaller as $L$ increases.

We define an "$n$-cluster configuration" as a string of $n$ clusters that occur consecutively (say in the clockwise direction in Fig. 1). We can describe such a configuration by giving the sizes of consecutive clusters using the notation $(x_1, x_2, \ldots, x_n)$. For instance, corresponding to the six clusters bracketed by the arrowheads drawn inside the circle of sites in Fig. 1, we have the six-cluster configuration (0,0,2,0,5,0). Given a $n$ cluster $(x_1, \ldots, x_n)$ and a fixed value of $i = 1, \ldots, n-1$ we define $P_n(x_1, \ldots, x_n)$ for $n \geqslant 2$ as the probability that a randomly chosen empty site is the one separating the clusters $x_i$ and $x_{i+1}$ in the configuration (note that this probability is the same for any choice of $i=1, \ldots, n-1$). For the special case $n=1$, we define $P_1(x)$ to be the probability that a randomly chosen empty site has a cluster of size $x$ on its clockwise side, which is the same as the probability that it has a cluster of size $x$ on its counterclockwise side. $P_1(x)$ is given by the number of clusters of size $x$ divided by the number of empty sites, i.e.,

$$P_1(x) = S_x/N_e. \tag{5}$$

$P_2(x,y)$ is the probability that a randomly chosen empty site separates the clusters of the two-cluster configuration $(x,y)$. For example, for the state shown in Fig. 1, we have $P_1(5) = 1/14$ and $P_2(0,2) = 4/14$. The probability distribution for

an $n-1$ cluster configuration, $P_{n-1}$, can be calculated as the marginal probability of $P_n$,

$$\sum_{x_n=0}^{L} P_n(x_1,\ldots,x_n) = P_{n-1}(x_1,\ldots,x_{n-1}). \tag{6}$$

In particular, for $n=2$ we have

$$\sum_{y=0}^{L} P_2(x,y) = P_1(x) = S_x/N_e. \tag{7}$$

Assuming statistical isotropy for $L \gg 1$, we postulate that $P_n(x_1,\ldots,x_n)$ is invariant to reflections of the grid, which implies that $P_n(x_1,\ldots,x_n)=P_n(x_n,\ldots,x_1)$.

### B. Continuous-time approximation

Our goal is to understand how $P_n$ evolves in time in situations far from the stationary state. We start with the following observations. When placing a tree on an empty site between a cluster of size $x$ and a cluster of size $y$ [i.e., a two-cluster configuration $(x,y)$], a new cluster of size $x+y+1$ is created by coalescing the two neighbors. In the special case when an empty site is surrounded by empty sites on both sides (i.e., $x=0$, $y=0$), the addition of a tree will create a cluster consisting of size one.

There are two possible ways for a cluster to change its size. It can either burn down or a tree can be added at its boundary. The probability that a cluster of size $x$ burns down in one step is $1-(1-f)^x$. We assume in what follows that $xf \ll 1$ so that

$$1-(1-f)^x \simeq xf. \tag{8}$$

The addition of a tree at one of the two empty sites on the cluster's boundary occurs with probability

$$1-(1-p)^2 \simeq 2p, \tag{9}$$

where we assume $p \ll 1$. Since $p$ and $xf$ are small, the probability that both of these events happen simultaneously (i.e., a tree is added to a cluster which burns down) is negligible compared to $p$ and $xf$. Similarly, the probability that we add two trees to the same cluster is of order $p^2$ and also can be neglected. According to Eqs. (8) and (9) the expected number of clusters of size $x$ that either become larger or burn down in one step is

$$S_x(x\gamma+2)p \quad (\text{for } p \ll 1, \gamma = f/p). \tag{10}$$

On the other hand, $S_x$ can grow if two neighboring clusters of sizes $x_1, x_2$ with $x=x_1+x_2+1$ coalesce, by the addition of a tree to the empty site that separates them. The expected number of such empty sites is $N_e \Sigma_{a+b+1=x} P_2(a,b)$, which combined with Eq. (10) gives the dynamical equation,

$$S_{x,m+1} - S_{x,m} = p_m N_{e,m} \sum_{a+b+1=x} P_2(a,b;m) - p_m(2+\gamma_m x)S_{x,m}, \tag{11}$$

where $x>0$ and $m$ denotes the model time step with $S_{x,m}$, $N_{e,m}$, and $P_2(a,b;m)$ the value of $S_x$, $P_2(a,b)$, and $N_e$ at time step $m$, and we now allow for time variation of $p$ and $\gamma$ via the replacements $p \to p_m$, $\gamma \to \gamma_m$. We approximate Eq. (11) for $p_m \ll 1$ by a continuous-time description using a scaled time variable,

$$t = \sum_{k=1}^{m} p_k, \tag{12}$$

and introducing the following notations, $S_{x,m}=S_x(t)$, $N_{e,m}=N_e(t)$, $p_m=p(t)$, $\gamma_m=\gamma(t)$, $P_n(x_1,\ldots,x_n;m)=P_n(x_1,\ldots,x_n;t)$, $dS_x(t)/dt=(S_{x,m+1}-S_{x,m})/p$. Thus Eq. (11) (which applies for $x>0$) becomes

$$\frac{dS_x(t)}{dt} = N_e(t) \sum_{a+b+1=x} P_2(a,b;t) - [2+\gamma(t)x]S_x(t). \tag{13}$$

$S_0(t)$ grows because clusters burn down and become smaller because empty sites become occupied,

$$\frac{dS_0(t)}{dt} = -2S_0(t) + \gamma(t)\sum_{y=1}^{L} y(y+1)S_y(t). \tag{14}$$

Summing $S_x(t)$ for all $x$'s according to Eq. (3) gives

$$\frac{dN_e(t)}{dt} = -N_e(t) + \gamma(t)\sum_{y} y^2 S_y(t). \tag{15}$$

As a check, we note that Eqs. (13) and (15) are consistent with the requirement of site conservation, which using Eq. (4) can be expressed as

$$\frac{d}{dt}\left(N_e(t) + \sum_{y} yS_y(t)\right) = 0. \tag{16}$$

Using $P_1(x;t)=S_x(t)/N_e(t)$, Eq. (13) can be rewritten in terms of probabilities,

$$\frac{d[N_e(t)P_1(x;t)]}{dt} = N_e(t) \sum_{a+b+1=x} P_2(a,b;t) - [2+\gamma(t)x]N_e(t)P_1(x;t), \tag{17}$$

which is the first step in a hierarchy of equations for $P_n$'s, to be discussed in the following section. Equations (13) and (15) describe the evolution of $S_x(t)$ if $P_2(a,b;t)$ is known. As we intend to give a general description of the model, we cannot assume $P_2(a,b;t)$ to be in its equilibrium form. In what follows we explain how a sequence of approximations can be obtained, with each step providing a more accurate description of the model.

### C. Estimation of $P_2(a,b;t)$

As a motivating example, we first consider the case where we start $t=0$ with a completely empty grid, i.e., $N_e(0)=S_0(0)=L$ and $S_x(0)=0$ for all $x>0$. We begin by assuming that the time elapsed since the start of the experiment is short enough that large clusters have not yet formed and that burning does not have a significant impact, i.e., $x\gamma \ll 1$. If the effect of fire is negligible, then the probabilities that any two sites are occupied are uncorrelated, and thus the probabilities of an empty site having a cluster of size $x$ on its left and a

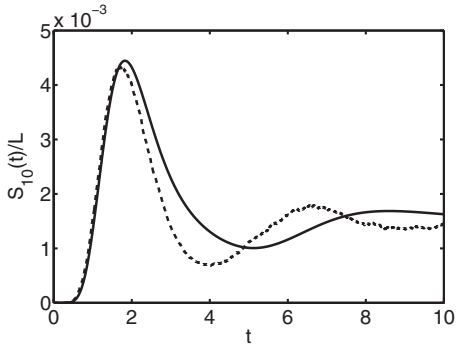


FIG. 2. $S_{10}/L$ versus time $t$ for $\gamma=5\times10^{-3}$ and $L=10^6$ with empty grid initial conditions. The dash-dotted curve is the result from a full numerical simulation, while the solid curve is from the solutions of Eqs. (15) and (19).

cluster of size $y$ on its right are independent. Hence

$$P_2(x,y;t) = P_1(x;t)P_1(y;t). \tag{18}$$

If we assume Eq. (18) to hold, then Eq. (13) takes the form

$$\frac{dS_x(t)}{dt} = \frac{1}{N_e(t)} \sum_{a+b+1=x} S_a(t)S_b(t) - [2+\gamma(t)x]S_x(t). \tag{19}$$

The time-dependent solution of Eq. (19) for $L \gg 1$ and $\gamma\Sigma_y y^2 S(y,t) \ll 1$ can be expressed explicitly as a function of $N_e(t)$ using a generating function technique as shown in the Appendix. Equation (19) combined with Eq. (15) determines the dynamics when $P_2(a,b;t)$ is approximately in the form (18). Eventually, clusters will grow so large that the assumed conditions under which Eq. (19) is valid will no longer be satisfied. To understand why this happens consider the situation when a large forest cluster burns down. This creates a long string of adjacent empty sites that will change the uniform distribution created by the slow driving input of tree growth, and Eq. (18) will no longer hold. At large time this effect will be more pronounced as we decrease the value of $\gamma$, since lowering $\gamma$ leads to larger time-asymptotic correlation length $\xi_c \sim \gamma^{-\nu}$ (see Ref. [18]). Figure 2 shows $S_{10}$ versus time with $\gamma=5\times10^{-3}$ and $L=10^6$ from a full numerical simulation of the FFM system (dotted curve) and from the solution of the approximating system equations (19) and (15) (solid curve). From such plots we find that the accuracy of Eq. (19) is relatively good for $\gamma=5\times10^{-3}$, if $t<2.5$. We will examine this in more detail in Sec. III.

We now turn to describe the dynamics of $P_2(x,y;t)$. The number of empty sites on the grid that separates the $x$ and $y$ clusters of the two-cluster $(x,y)$ is $N_e(t)P(x,y;t)$. A two cluster $(x,y)$ can be created in one step by adding a tree to appropriate three-clusters: As shown in Fig. 3, the two cluster $(x,y)$ will be created from $(a,b,y)$ or $(x,a,b)$ if a tree is grown in the empty site separating the $a$ and $b$ clusters and if $a+b+1=x$ in the first case or if $a+b+1=y$ in the second case. According to its definition $P_3(u,v,w;t)$ is the probability that a randomly chosen empty site is the one separating the $u$ and $v$ clusters (which is the same as the probability that

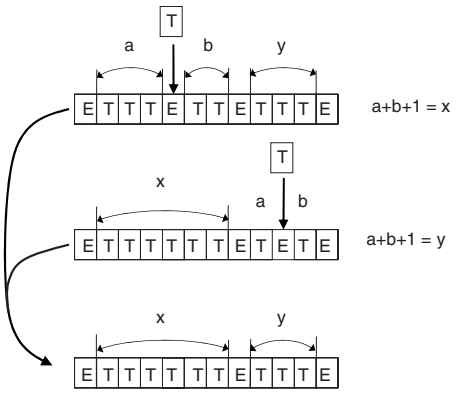


FIG. 3. Two clusters are created by coalescing three-cluster configurations.

it separates the $v$ and $w$ clusters) in the three cluster $(u,v,w)$. Accordingly, the expected number of configurations of type $(x,y)$ created by tree growth in one step is

$$\sum_{a+b+1=y} p(t)N_e(t)P_3(x,a,b;t) + \sum_{a+b+1=x} p(t)N_e(t)P_3(a,b,y;t). \tag{20}$$

On the other hand, the number of two-cluster configurations $(x,y)$ decreases if either a tree is added to any of the three empty sites bounding $x$ and/or $y$ (these three empty sites are the one to the left of the $x$ cluster, the one between the $x$ and $y$ clusters, and the one to the right of the $y$ cluster). As a result, the expected number of two clusters of type $(x,y)$ destroyed because of the addition of trees is $3p(t)N_e(t)P_2(x,y;t)$. Finally, fires can destroy either $x$ or $y$ in a configuration $(x,y)$, which decreases the number of $(x,y)$ two clusters by $p(t)\gamma(t)N_e(t)P_2(x,y;t)(x+y)$. Summarizing, we have

$$\begin{aligned}\frac{d[N_e(t)P_2(x,y;t)]}{dt} &= -[3+\gamma(t)(x+y)]N_e(t)P_2(x,y;t) \\ &+ \sum_{a+b+1=x} N_e(t)P_3(a,b,y;t) \\ &+ \sum_{a+b+1=y} N_e(t)P_3(x,a,b;t)\end{aligned} \tag{21}$$

for $(x>0, y>0)$. Thus the solution of $P_2$ depends on $P_3$ [similar to the dependence of the evolution of $P_1$ on $P_2$ in Eq. (17)]. We have to consider the case when either $x=0$ or $y=0$ separately, because clusters of type $(0,x)$ will have positive contribution from all clusters of type $(a,x)$, $a>0$ if $a$ burns down. If $x=0$ and $y>0$ then we have to add $\Sigma_a N_e(t)P_2(a,x;t)a\gamma(t)$ to the right side of Eq. (21), which yields

$$\begin{aligned}\frac{d[N_e(t)P_2(0,y;t)]}{dt} &= -[3+\gamma(t)y]N_e(t)P_2(0,y;t) \\ &+ \sum_{a+b+1=y} N_e(t)P_3(0,a,b;t) \\ &+ \sum_{a} N_e(t)P_2(a,y;t)a\gamma(t).\end{aligned} \tag{22}$$

The equation for $N_e(t)P_2(0,0;t)$ can be obtained if we combine Eqs. (21) and (22) with the normalizing condition $\Sigma_{x,y}P_2(x,y;t)=1$. It can be shown that Eqs. (21) and (22) are consistent with our previous dynamical equation, Eq. (13), using Eq. (6).

We can similarly continue this sequence of equations, e.g., the dynamics of $N_eP_n$ for $x_i>0$ $(i=1,2,\ldots,n)$ is given by

$$\frac{d[N_e(t)P_n(x_1,\ldots,x_n)]}{dt} = -\left[n+1+\gamma(t)\left(\sum_{i=1}^{n}x_i\right)\right]N_e(t)P_n(x_1,\ldots,x_n;t) + N_e(t)\sum_{j=1}^{n}\sum_{a+b=x_j}P_{n+1}(x_1,\ldots,x_{j-1},a,b,x_{j+1},\ldots,x_n;t), \tag{23}$$

where in the sum over $j$ we define the first and last terms of the sum ($j=1$ and $j=n$) so that the argument of $P_{n+1}$ is $(a,b,x_2,\ldots,x_n)$ for $j=1$ and $(x_1,\ldots,x_{n-1},a,b)$ for $j=n$. Thus we obtain a sequence of descriptions in which the evolution of $P_n(x_1,x_2,\ldots,x_n;t)$ depends on the higher-order probability functions $P_{n+1}(x_1,x_2,\ldots,x_{n+1};t)$. We can truncate the resulting equation for a given $P_n(x_1,x_2,\ldots,x_n;t)$ by making the assumption that for an $(n+1)$-cluster configuration of type $(x_1,\ldots,x_{n+1})$ the probability distribution of $x_1$ does not depend on $x_{n+1}$, which can be stated in terms of conditional probabilities,

$$\tilde{P}_{n+1}(x_1|x_2,\ldots,x_{n+1};t)\cong\tilde{P}_n(x_1|x_2,\ldots,x_n;t). \tag{24}$$

This supposition is equivalent to assuming a limited correlation length and is supported by the numerical observation that, in the statistically steady state, the correlation function decays exponentially with the distance [18]. Relationship (24) along with Bayes' theorem can be used to obtain

$$P_{n+1}(x_1,\ldots,x_{n+1};t)=\tilde{P}_{n+1}(x_1|x_2,\ldots,x_{n+1};t)P_n(x_2,\ldots,x_{n+1};t) \cong \tilde{P}_n(x_1|x_2,\ldots,x_n;t)P_n(x_2,\ldots,x_{n+1};t), \tag{25}$$

where we have used Eq. (24) to approximate $\tilde{P}_{n+1}$ by $\tilde{P}_n$. Now again using Bayes' theorem we have $\tilde{P}_n(x_1|x_2,\ldots,x_n;t)P_{n-1}(x_2,\ldots,x_n)=P_n(x_1,\ldots,x_n;t)$, which we use to eliminate $\tilde{P}_n$ in Eq. (25), resulting in

$$\frac{P_n(x_1,\ldots,x_n;t)P_n(x_2,\ldots,x_{n+1};t)}{P_{n-1}(x_2,\ldots,x_n;t)}, \tag{26}$$

and $P_{n-1}$ can be expressed in terms of $P_n$ by the use of Eq. (6), $P_{n-1}(x_2,\ldots,x_n;t)=\Sigma_{x_1}P_n(x_1,\ldots,x_n;t)$. The importance of Eq. (26) is that it expresses $P_{n+1}$ as a function of lower-order probabilities $P_n$ and $P_{n-1}$, which combined with the dynamical equations, e.g., Eq. (23), gives a closed set of first-order ordinary differential equations. The highest-order approximation we will examine in the following section is given by Eqs. (21) and (22). In this case we close our hierarchy of equations with

$$P_3(a,b,c;t)=\frac{P_2(a,b;t)P_2(b,c;t)}{P_1(b;t)}. \tag{27}$$

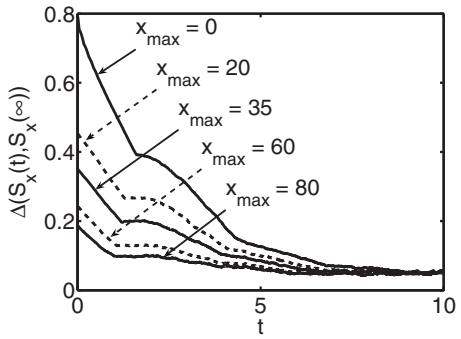


FIG. 4. Difference between the perturbed and time-asymptotic distributions for different initial conditions with $\gamma=5\times10^{-3}$ and $L=10^6$.

## III. NUMERICAL EXPERIMENTS

### A. Relaxation time

We introduce a measure characterizing the difference between two cluster size distributions, $S_x$ and $S_x^*$,

$$\Delta(S_x,S_x^*)=\left(|N_e-N_e^*|+\sum_{x=0}^{L}|S_x-S_x^*|x\right)\Big/(2L). \tag{28}$$

By Eq. (4) we have that $0\leqslant\Delta\leqslant1$. As an indication of how the system relaxes to its time asymptotic steady state when $\gamma$ is time independent, Fig. 4 shows plots of $\Delta(S_x(t),S_x(\infty))$ versus $t$, where $S_x(t)$ is calculated from the FFM with different initial conditions, and $S_x(\infty)$ is calculated as an average over a long time interval $[t_1,t_2]$, where $t_1$ is large. In particular, as initial conditions for calculating $S_x(t)$ we took the steady-state solution $S_x(\infty)$ of the FFM and eliminated clusters that were larger then a chosen cutoff value $x_{\max}$. In other words, if an occupied site belongs to a cluster of size $x\geqslant x_{\max}$, we replace that occupied site by an empty site.

We see from Fig. 4 that for a fixed $\gamma$, a broad range of perturbations agree in the order of magnitude in their relaxation time scales as measured by $\Delta$. Because $\Delta$ involves an average over all $x$, we refer to the relaxation of $\Delta$ as a "global relaxation." Later (in Sec. III C) we will examine the relaxation of $S_x$ as a function of $x$, and will find $x$-dependent "local" time scales. Again referring to Fig. 4, we note that, because of statistical fluctuations, none of the curves converge to exactly zero. For the chosen $\gamma$ and system size of $L=10^6$ used in Fig. 4, the statistical fluctuation between the time-asymptotic $S_x(t)$ and $S_x(\infty)$ is around $\Delta\approx8\times10^{-2}$. As a comparison, $L=10^5$ results in $\Delta=0.13$ and $L=10^7$ leads to $\Delta=2.2\times10^{-2}$. According to our observations, for a fixed grid size $L$, the lower $\gamma$, the higher the level of statistical fluctuations. In particular, if $\gamma$ is too small, e.g., $\gamma<10^{-4}$ for $L=10^6$, the effect of fluctuations of $S_x(t)$ becomes so large that it is comparable in magnitude to $S_x(t)$ itself.

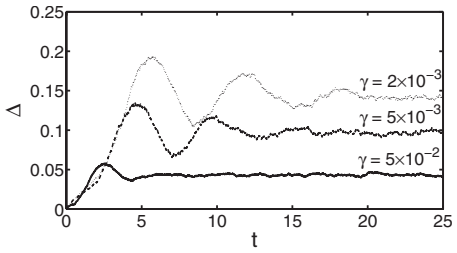


FIG. 5. The accuracy parameter $\Delta$ versus time with $L=10^6$ and $\gamma=5\times10^{-2}$, $5\times10^{-3}$, $2\times10^{-3}$ for the second-order approximations (21) and (22).

### B. Accuracy of our approximate descriptions of FFM dynamics

To assess the accuracy of our analytical considerations, we now compare the dynamics predicted by Eqs. (21), (22), and (19) with time-independent $\gamma$ to full numerical simulations of the FFM. For the solution of the full FFM we used a grid size $L=10^6$, with $p=5\times10^{-4}$ and $f=p\gamma$, with $\gamma=5\times10^{-2}$, $5\times10^{-3}$, $2\times10^{-3}$, $5\times10^{-5}$. For the numerical solution of Eqs. (21) and (22) we proceed as follows. Equations (21) and (22) determine the time evolution of the probability function $P_2(x,y;t)$, which at each time $t$ depends on the variables $x$ and $y$. Thus we have to solve the equations on a two-dimensional grid of size $L\times L$. However, it is known from the statistically steady solution of the full FFM [9], that for a given $\gamma$ there exists a size limit above which forest clusters are extremely rare. Therefore, instead of solving Eqs. (21) and (22) for all clusters sizes, between 0 and $L=10^6$, we restrict our attention to the most frequently occurring ones and solve Eqs. (21) and (22) on a two-dimensional grid $(x,y)$ of size $500\times500$.

Equation (13) is the first in our hierarchy of equations and therefore from now on we will refer to it as the first-order approximation. Similarly, the dynamics determined by Eqs. (21) and (22) will be called the second-order approximation. Figure 5 shows $\Delta(S_x(t),S_x^*(t))$ versus $t$ for three different values of $\gamma$ versus $t$, where $S_x(t)$ is obtained from the second-order approximation and $S_x^*(t)$ is the result from numerical solution of the FFM. For both, the initial condition was an empty grid [i.e., $N_e(0)=S_0(0)=L$ and $S_x(0)=0$ for $x\geqslant1$]. It is seen that, if $\Delta(t)$ at large time (denoted $\Delta_\infty$) is larger for one value of $\gamma$ than for another, then this is generally also true for

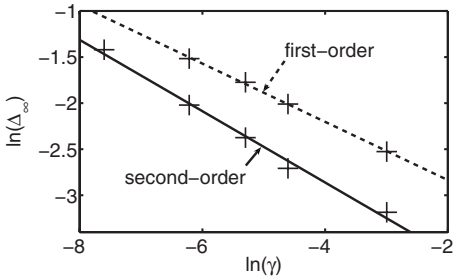


FIG. 6. The accuracy parameter $\Delta_\infty$ versus the forest-fire intensity $\gamma$, for the second-order model given by Eqs. (21) and (22) (solid curve) and for the first-order model given by Eq. (19) (dashed curve). $L=10^6$.

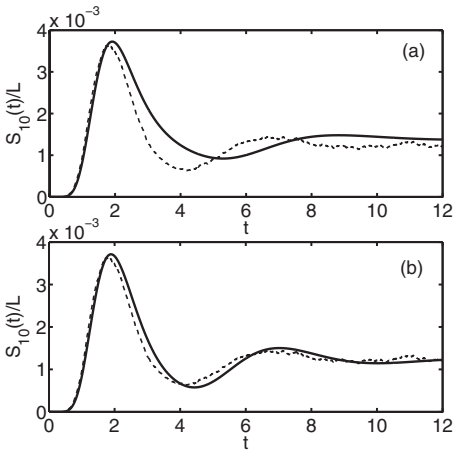


FIG. 7. $S_{10}$ versus time $t$ for $\gamma=5\times10^{-3}$ and $L=10^6$ with empty grid initial conditions. The dotted curves are the results from a full numerical simulation of the FFM, while the solid curves in (a) and (b) correspond, respectively, to the first- and second-order approximations.

$\Delta$ at other times. Thus we characterize the overall accuracy by $\Delta_\infty$. Figure 6 shows $\Delta_\infty$ versus $\gamma$ for the first- and second-order approximations. We note that statistical fluctuations account for some of the difference between the $S_x$ and $S_x^*$. It is apparent that the second-order approximation performs significantly better than the first-order approximation. Our results also indicate that decreasing $\gamma$ increases $\Delta_\infty$. The log-log plot shown in Fig. 6 demonstrates that $\Delta_\infty$ versus $\gamma$ is consistent with a power-law dependence,

$$\Delta_\infty \sim \gamma^{-a} \tag{29}$$

for both the second-order approximation $a\simeq0.38$, and the first-order approximation $a\simeq0.31$. Figure 7 compares the time dependence of $S_{10}(t)$ from the full FFM with the time dependence obtained from the first-order approximation [solid curve in Fig. 7(a)] and from the second-order approximation [solid curve in Fig. 7(b)]. The second-order method predicts the time dependence of the evolution [Fig. 7(b)] and the time-asymptotic form of $S_x$ very well. Figure 8 shows the time-asymptotic cluster size distribution $S_x(\infty)$ versus $x$ obtained from solution of our second-order equations (solid

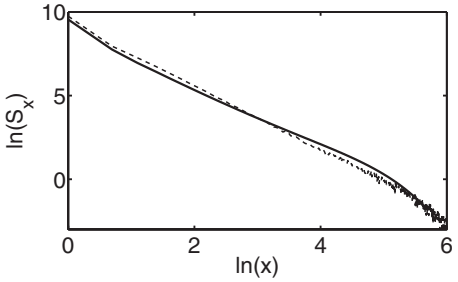


FIG. 8. The time-asymptotic $\ln(S_x)$ versus $\ln(x)$. The dotted curve is the result from a full numerical simulation of the FFM, while the solid curve is from the second-order approximation. The parameter values are $\gamma=5\times10^{-3}$, $L=10^6$.

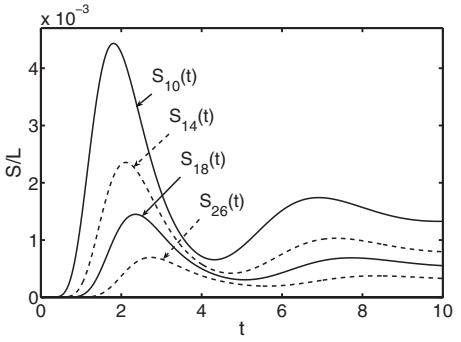


FIG. 9. $S_x$ versus time $t$ for $\gamma=5\times10^{-3}$, $L=10^6$, and $x=10,14,18,26$ for the second-order approximation with empty grid initial conditions.

curve) and from a numerical calculation of the full FFM (dots). Again we see very good agreement.

### C. Cluster-size-dependent dynamics

We now examine how the relaxation dynamics of $S_x(t)$ for time-independent $\gamma$ depends on the cluster size $x$. Figure 9 shows $S_x(t)$ from the second-order approximation with empty grid initial conditions for cluster sizes $x=10,14,18,24$. When the FFM evolves, starting with a completely empty grid as the initial condition, the first maximum that $S_x(t)$ reaches will also be its global maximum in time, as shown in Fig. 7. From Fig. 9 it is apparent that larger clusters reach this maximum later in time. This can be interpreted as being due to the extra time taken by the coalescence process that creates larger clusters form smaller ones. In the absence of forest fires, i.e., $\gamma=0$, $S_x(t)$ would relax to $S_x(t)=0$ for $x<L$, after this maximum is reached, as seen from the analytical solution presented in the Appendix. In the presence of forest fires, however, $S_x(t)$ oscillates around its time asymptotic value until complete relaxation is achieved.

We examine the accuracy of the first-order approximation's ability to predict the time of the first maximum of $S_x(t)$. For every cluster size $x$ we define $t_{\max}(x)$ to be the time instant when $S_x$ reaches its first maximum value. An approximate analytical expression $t_{\max}\approx\ln(x/2+1)$ is obtained in the Appendix. Thus the characteristic time scale for evolution of $S_x$ as characterized by $t_{\max}$ is predicted to be longer for larger $x$ (i.e., larger cluster sizes). Figure 10 compares the

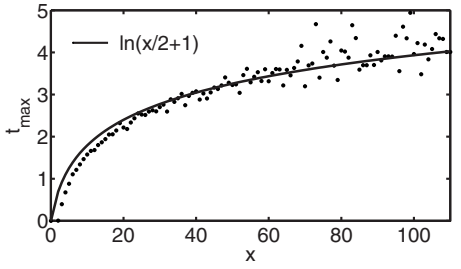


FIG. 10. $t_{\max}(x)$ versus $x$ for $\gamma=5\times10^{-3}$, $L=10^6$. The dots are the results from a full numerical simulation of the FFM, while the solid curve is the analytical result from the first-order approximation, i.e., $t_{\max}(x)=\ln(x/2+1)$ [Eq. (A4)].

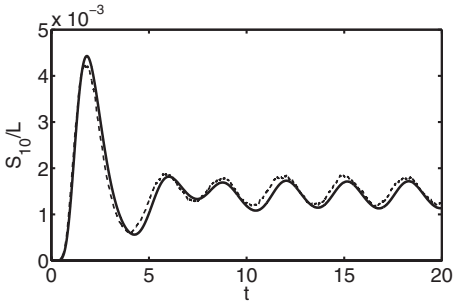


FIG. 11. $S_{10}/L$ versus $t$ for $\gamma_0=5\times10^{-3}$, $L=10^6$, $\omega=1$, and $A=0.5$. The dotted curve is the result from the FFM, while the solid curve is from the second-order approximation.

calculated and the analytical $t_{\max}(x)$ data for $\gamma=5\times10^{-3}$. We see that the full FFM simulation results for $t_{\max}$ are in good agreement with our first-order approximation.

### D. Dynamics for time-dependent $\gamma(t)$

As a final experiment we examine the ability of our second-order approximation to describe the behavior of the FFM when $\gamma(t)$ depends on time. For our experiment we chose

$$\gamma(t)=\gamma_0[1+A\sin(\omega t)] \quad \text{with } A<1, \tag{30}$$

with $\gamma_0=5\times10^{-3}$. We explore the dependence of our results on the driving amplitude $A$ and frequency $\omega$. Consistent with our expectation, we found that, after the transients related to initial conditions relax, $S_x(t)$ shows temporally periodic oscillatory behavior at the frequency $\omega$, $S_x(t)=S_x(t+2\pi/\omega)$, as shown in Fig. 11. $S_x(t)$ has an approximately sinusoidal time dependence for sufficiently small amplitudes and large frequencies, e.g., if $A=0.5$, and $\omega=1$, as shown in Fig. 11. With the increase of the driving amplitude and lowering of the frequency, this sinusoidal wave form is distorted. For cases where $S_x(t)$ is approximately sinusoidal, we find that the amplitude of the oscillation of $S_x$, denoted $a(x)$, has an approximate power-law dependence on the cluster size $x$, i.e., $a(x)\sim x^{-\alpha}$, with an exponent $\alpha\simeq1.56$ (see Fig. 12), and the midpoint of the oscillation is, to within our available accuracy, the same as for the equilibrium solution of the FFM with $\gamma(t)$ set to a steady value $\gamma_0$. The dependence of $a(1)$ on the driving frequency $\omega$ is shown in Fig. 13. The maximum am-

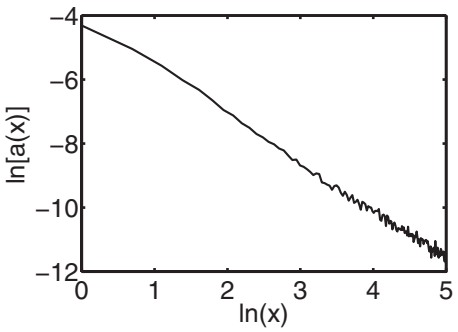


FIG. 12. The amplitude of oscillation $a(x)$ versus the cluster size $x$ for $\gamma_0=5\times10^{-3}$, $L=10^6$, $\omega=1$, and $A=0.5$.

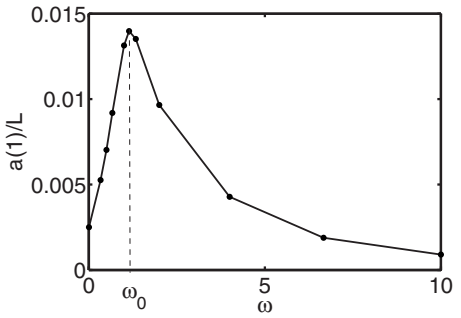


FIG. 13. $a(1)/L$ versus $\omega$ for the second-order approximation ($\omega_0 \approx 1.14$). Parameter values are $\gamma=5\times10^{-3}$, $L=10^6$, and $A=0.5$.

plitude of $a(x)$ for each cluster size $x$ is attained at the resonant frequency $\omega_0 \simeq 1.14$. In the limit $\omega \to 0$ the system adiabatically oscillates among steady-state solutions corresponding to different constant $\gamma$ values. In other words, if we denote the steady-state solution corresponding to a fixed value of $\gamma$ by $S_x(\infty,\gamma)$ then $S_x(t) \simeq S_x(\infty,\gamma(t))$ for $\omega \ll \omega_0$, which for $A=0.5$ and $\gamma_0=5\times10^{-3}$ leads to a nonvanishing oscillation amplitude $a(1)=2.5\times10^{-3}$.

The existence of the resonant frequency is due to the presence of a characteristic time scale in the steady state, denoted $T$, which is defined as the average time needed for an empty site to become occupied and empty again. In order to give an estimate for $T$, consider the following. The probability that an empty site becomes occupied after time $t$ equals $1-e^{-t}$, leading to an average time for tree growth 1. If $N_e$ denotes the number of empty sites in the steady state, then the number of trees grown on the grid in one time step is $N_e p$, which equals the number of trees destroyed. Therefore, the fraction of trees destroyed in one time step is $pN_e/(L-N_e)$. Assuming a constant rate of destruction for all trees, the probability that a tree burns down after time $t$ equals $1-\exp[-tN_e/(L-N_e)]$, leading to an average lifetime $(L-N_e)/N_e$. As a result, we have $T=1+(L-N_e)/N_e=1/(N_e/L)$, which corresponds to the frequency $\omega=2\pi N_e/L \approx 1.07$, using the measured result $N_e/L \simeq 0.17$ for $\gamma=5\times10^{-3}$. Resonance occurs when we drive the system at a frequency corresponding the characteristic time scale.

We define a phase shift $\Delta\phi(x)$ by which the oscillation of $S_x(t)$ lags that of $\gamma(t)$. Figure 14 shows $\Delta\phi(x)$ versus the

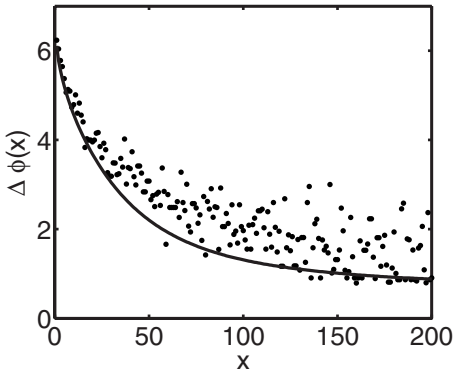


FIG. 14. $\Delta\phi(x)$ versus $x$. The solid curve is for the second-order approximation. Dots correspond to the full FFM. Parameter values are $\gamma=5\times10^{-3}$, $L=10^6$, $\omega=1$, and $A=0.5$.

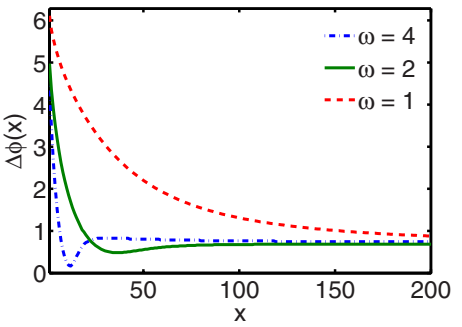


FIG. 15. (Color online) $\Delta\phi(x)$ versus $x$ for the second-order approximation. Parameter values are $\gamma_0=5\times10^{-3}$, $L=10^6$, $\omega=1,2,4$, and $A=0.5$.

cluster size $x$, with the solid curve corresponding to the second-order approximation and the dots to the full FFM. Burning of large clusters simultaneously creates many zero size clusters, therefore zero size clusters oscillate close in phase to larger ones seen illustrated in Fig. 14 (note that $\Delta\phi=0$ and $\Delta\phi=2\pi$ are equivalent). Furthermore, in the region of large burns, small size clusters begin to form through tree growth and coalesce in time to form larger clusters, leading to the decrease of $\Delta\phi$ with increasing $x$ (seen in Fig. 14). Figure 15 shows $\Delta\phi$ as a function of cluster size $x$, obtained from the second-order approximation, for the frequencies $\omega=1,2,4$. An important point is that for $\omega>1.5$ the phase difference $\Delta\phi(x)$ has a local minimum. Figure 16 shows $S_{10}$ versus $S_6$ starting from empty grid initial conditions as obtained from the second-order approximation [Fig. 16(a)] and from the full FFM [Fig. 16(b)]. From both we see the effect of the difference between $\Delta\phi(10)$ and $\Delta\phi(6)$ as manifested by the elliptical shape of the trajectory $S_{10}(t)$ versus $S_6(t)$, and that the oscillation of $S_6(t)$ leads that of $S_{10}(t)$, $\Delta\phi(10)>\Delta\phi(6)$ consistent with Fig. 14.

## IV. CONCLUSION

In this paper we examined *dynamical* behavior of the self-organized forest-fire model in one dimension, on a time scale that is faster than, or of the order of the time needed for relaxation of the system to the statistically steady state. We found that, similarly to the statistically steady-state behavior,

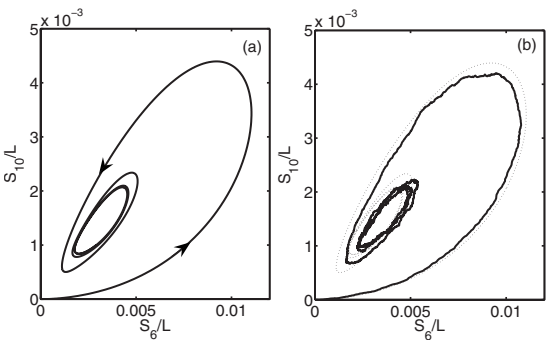


FIG. 16. $S_{10}$ versus $S_6$ for $\gamma_0=5\times10^{-3}$, $L=10^6$, $\omega=1$, and $A=0.5$ for the second-order approximation (a) and the FFM (b). The dotted curve in (b) corresponds to the second-order approximation.

the parameter $\gamma$ plays a crucial role in determining the dynamics. From a computational point of view, we found that for a given grid size $L$, decreasing $\gamma$ increases the effect of statistical fluctuations, which makes the study of the dynamical behavior via solution of the full FFM less effective. This becomes even more pronounced for larger cluster sizes. As an alternative, we introduced an analytical approach, based on a hierarchy of equations, which correspond to the $L\to\infty$ limit of the FFM. The closure scheme for this hierarchy, which is equivalent to assuming a limited correlation length, gives a set of self-consistent, successively more accurate approximations to the dynamics. The agreement between our hierarchy of equations and the numerical solutions of the full FFM depends on the forest fire intensity $\gamma$. Since a decrease of $\gamma$ leads to larger correlation length [18], in order to accurately treat smaller lighting intensities $\gamma$, one would have to go to higher-order approximations in our hierarchy. We found very good agreement between our second-order approximation and numerical simulations of the FFM for $\gamma \geqslant 2\times 10^{-3}$.

The relaxation of the FFM to its time-asymptotic value, measured by the distance between distributions [in the sense (28)], can be characterized by a single relaxation time scale over a range of initial conditions (for a fixed $\gamma$). Relaxation measured by Eq. (28) characterizes the process in a global sense. On the other hand, locally for each individual cluster size, a cluster-size-dependent time scale exists. We examined this effect, starting from empty grid initial conditions, and found that the time at the occurrence of the first maximum of $S_x(t)$ has an approximate logarithmic dependence on the cluster size. This is due to the fact that larger clusters are created through a cascading process from smaller ones, leading to a time delay.

To examine the effect of temporally changing external conditions on the FFM, we investigated the effect of a time-dependent forest-fire intensity $\gamma(t)$. We found that for a sinusoidal $\gamma(t)$, that (i) the numbers of clusters of size $x$, $S_x(t)$, oscillates at the same frequency as $\gamma(t)$; (ii) the amplitude of the oscillation is a power-law function of the cluster size; and (iii) there is a cluster-size-dependent phase lag.

## ACKNOWLEDGMENTS

This work was supported by grants from the NSF (Grant No. PHYS0456240) and the ONR (Physics).

## APPENDIX

For $L\gg 1$, $\gamma$ constant and $\gamma\Sigma_y y^2 S(y,t)\ll 1$ the solution of Eq. (19) can be given by introducing $F(x,t)=S_x(t)e^{-(2+\gamma x)t}$,

$$\frac{dF(x,t)}{dt}=\frac{e^{-(2-\gamma)t}}{N_e(t)}\sum_{a+b+1=x}F(a,t)F(b,t). \tag{A1}$$

Equation (A1) can be explicitly solved for the generating function $G(z,t)=\Sigma_{y=0}^{L}z^y F(y,t)$,

$$G(z,t)=\frac{G(z,0)}{1-zG(z,0)\displaystyle\int_0^t e^{-(2-\gamma)\tau}/N_e(\tau)d\tau}. \tag{A2}$$

In particular, for empty grid initial condition [i.e., $G(z,0)=L$], Eq. (A2) yields

$$S_x(t)=L\left(\frac{1-e^{-(1-\gamma)t}}{1-\gamma}\right)^x e^{-(2+\gamma x)t},$$

$$N_e(t)=Le^{-t}. \tag{A3}$$

Accordingly, $t_{\max}$, defined in Sec. III $[dS_x(t_{\max})/dt=0]$, can be approximated as

$$t_{\max}(x)\approx \ln\left(\frac{x}{2}+1\right), \tag{A4}$$

and the the magnitude of the first maximum is

$$S_{\max}(x)=S_x(t_{\max})\approx\frac{4x^x}{(x+2)^{x+2}}. \tag{A5}$$

[1] P. Bak, C. Tang, and K. Wiesenfeld, Phys. Rev. Lett. **59**, 381 (1987); Phys. Rev. A **38**, 364 (1988).
[2] L. P. Kadanoff, S. R. Nagel, L. Wu, and S. M. Zhou, Phys. Rev. A **39**, 6524 (1989).
[3] D. Dhar, Phys. Rev. Lett. **64**, 1613 (1990).
[4] Z. Olami, Hans Jacob S. Feder, and K. Christensen, Phys. Rev. Lett. **68**, 1244 (1992).
[5] T. A. Witten and L. M. Sander, Phys. Rev. Lett. **47**, 1400 (1981).
[6] D. Wilkinson and J. F. Willemsen, J. Phys. A **16**, 3365 (1983).
[7] M. Paczuski, S. Boettcher, and M. Baiesi, Phys. Rev. Lett. **95**, 181102 (2005).
[8] P. Bak, K. Chen, and C. Tang, Phys. Lett. A **147**, 297 (1990).
[9] B. Drossel and F. Schwabl, Phys. Rev. Lett. **69**, 1629 (1992).
[10] P. Grassberger, J. Phys. A **26**, 2081 (1993).
[11] B. Drossel, Phys. Rev. Lett. **76**, 936 (1996).
[12] B. Drossel, S. Clar, and F. Schwabl, Phys. Rev. Lett. **71**, 3739 (1993).
[13] K. Christensen, H. Flyvbjerg, and Zeev Olami, Phys. Rev. Lett. **71**, 2737 (1993).
[14] D. L. Turcotte, B. D. Malamud, G. Morein, and W. I. Newman, Physica A **268**, 629 (1999).
[15] V. Loreto, L. Pietronero, A. Vespignani, and S. Zapperi, Phys. Rev. Lett. **75**, 465 (1995).
[16] A.-L. Barabasi and R. Albert, Science **286**, 509 (1999).
[17] M. Paczuski and P. Bak, Phys. Rev. E **48**, R3214 (1993).
[18] A. Honecker and I. Peschel, Physica A **239**, 509 (1997).
[19] S. Clar, B. Drossel, and F. Schwabl, J. Phys.: Condens. Matter **8**, 6803 (1996).